/12/8205-898–909$25.00
MOLECULAR PHARMACOLOGY
Vol. 82, No. 5
80630/3800743

Mol Pharmacol 82:898–909, 2012

A Second Extracellular Site Is Required for Norepinephrine Transport by the Human Norepinephrine Transporter[S]

Ching-I A. Wang, Nausad H. Shaikh, Soumya Ramu, and Richard J. Lewis

Institute for Molecular Bioscience, The University of Queensland, St. Lucia, Brisbane, Queensland, Australia

Received June 12, 2012; accepted July 30, 2012

ABSTRACT

The human norepinephrine transporter (NET) is implicated in many neurological disorders and is a target of tricyclic antidepressants and nisoxetine (NX). We used molecular docking simulations to guide the identification of residues likely to affect substrate transport and ligand interactions at NET. Mutations to alanine identified a hydrophobic pocket in the extracellular cavity of NET, comprising residues Thr80, Phe317, and Tyr317, which was critical for efficient norepinephrine (NE) transport. This secondary NE substrate site (NESS-2) overlapped the NX binding site, comprising Tyr84, Phe317, and Tyr317, and was positioned ~11 Å extracellular to the primary site for NE (NESS-1). Thr80 in NESS-2 appeared to be critical in positioning NE for efficient translocation to NESS-1. Three residues identified as being involved in gating the reverse transport of NE (Arg81, Gln314, and Asp473) did not affect NE affinity for NESS-1. Mutating residues adjacent to NESS-2 abolished NET expression (D75A and L76A) or appeared to affect NET folding (S419A), suggesting important roles in stabilizing NET structure, whereas W308A and F388A at the top of NESS-2 abolished both NE transport and NX binding. Our findings are consistent with a multistep model of substrate transport by NET, for which a second, shallow extracellular NE substrate site (NESS-2) is required for efficient NE transport by NET.

Introduction

Intracellular communication between neurons in the central nervous system is critically dependent on the controlled release of neurotransmitters at synapses. Monoamine transporters are members of SLC6 family of neurotransmitter sodium symporters (NSSs) that use the Na^+ and Cl^- electrochemical gradient to actively remove (transport) biogenic monoamines, including dopamine, norepinephrine (NE), and serotonin, from the synapse cleft and back into the nerve terminal (Masson et al., 1999; Chen et al., 2004). Consistent with their crucial role in regulating the strength and duration of synaptic transmission, malfunction or altered expression levels of monoamine transporters are implicated in a number of psychiatric and neurological disorders, including Parkinson's disease (Kim et al., 1997), Wilson's disease (Jeon et al., 1998), Lesch-Nyhan disease (Wong et al., 1996), attention deficit hyperactivity disorder (Dougherty et al., 1999), and major depression (Klimek et al., 1997). Moreover, monoamine transporters have been shown to be a primary target for the psychostimulants cocaine (Ritz et al., 1987) and amphetamine (Amara and Sonders, 1998), as well as tricyclic antidepressants (TCAs) and analgesic venom peptides (Sharpe et al., 2001; Nielsen et al., 2005; Brust et al., 2009).

Extensive pharmacological and biochemical studies, in conjunction with three-dimensional comparative modeling, have helped characterize the substrate permeation pathway of monoamine transporters and the structural features contributing to substrate and ligand selectivity. However, only since the structure of a related bacterial (*Aquifex aeolicus*) leucine transporter ($LeuT_{Aa}$) was solved (Yamashita et al., 2005) has it been possible to start to develop a detailed molecular view of these interactions. The $LeuT_{Aa}$ crystal structures in complex with substrate leucine (Yamashita et al., 2005) revealed that one leucine and two Na^+ ions were buried in an occluded conformation that was proposed to be a transition state between the open-to-out (substrate binding)

This research was supported by the Australian Research Council [Discovery Grant DP120101992] and National Health and Medical Research Council Program [Grant 569927] (to R.J.L.).

C.-I.A.W. and N.H.S. contributed equally to this work.

Article, publication date, and citation information can be found at http://molpharm.aspetjournals.org.
http://dx.doi.org/10.1124/mol.112.080630.

[S] The online version of this article (available at http://molpharm.aspetjournals.org) contains supplemental material.

ABBREVIATIONS: NSS, neurotransmitter sodium symporter; NE, norepinephrine; TCA, tricyclic antidepressant; $LeuT_{Aa}$, *Aquifex aeolicus* leucine transporter; SSRI, selective serotonin reuptake inhibitor; NSS, neurotransmitter sodium symporter; SERT, serotonin transporter; DAT, dopamine transporter; GAT, GABA transporter; NET, norepinephrine transporter; NX, nisoxetine; NESS, norepinephrine substrate site; TMH, transmembrane helix; EL, extracellular loop; 3D, three-dimensional; hNET, human norepinephrine transporter; RMSD, root mean square deviation; PAGE, polyacrylamide gel electrophoresis.

and open-to-in (substrate releasing) conformations of the alternating access model of transport (Krishnamurthy et al., 2009). The determination of three $LeuT_{Aa}$-TCA cocrystal structures (Singh et al., 2007; Zhou et al., 2007) and three $LeuT_{Aa}$-selective serotonin reuptake inhibitor (SSRI) structures (Zhou et al., 2009) revealed an extracellular antagonist binding site S2, ~11Å above the leucine binding site S1, consistent with noncompetitive inhibition of leucine by TCAs in $LeuT_{Aa}$ (Singh et al., 2007). More recently, Krishnamurthy and Gouaux (2012) successfully trapped $LeuT_{Aa}$ in substrate-free open-to-out and open-to-in conformations using conformation-specific antibody fragments. Together with the substrate-bound conformation (Yamashita et al., 2005), this work has defined the structural basis for the alternating access mechanism of the NSS.

In separate studies, the Javitch group have identified a second high-affinity substrate binding site in $LeuT_{Aa}$ at the position overlapping the S2 site, using steered molecular dynamics in combination with single amino acid imaging (alanine) (Zhao et al., 2011), radiotracer binding and flux experiments (Shi et al., 2008), and equilibrium dialysis with S1- and S2-impaired $LeuT_{Aa}$ mutants (Quick et al., 2012). In these studies, a 2:1 stoichiometry between leucine and $LeuT_{Aa}$ is observed and both the S1 and S2 sites can be occupied simultaneously. The Javitch group further demonstrated the pivotal involvement of the S2 site in substrate transport by introducing mutations at S2 (Shi et al., 2008) or blocking S2 with TCAs (Shi et al., 2008) and the commonly used crystallization detergent octylglucoside (Quick et al., 2009), seen in $LeuT_{Aa}$ crystal structures (Singh et al., 2007, 2008). Based on these data, this group has proposed a modified hypothesis in which the alternating access mechanism is initiated when a second leucine binds to S2 and triggers a conformational change to open-to-in, allowing release of a leucine already bound to S1. Despite considerable effort to resolve this point of difference (Piscitelli et al., 2010; Quick et al., 2012; Wang et al., 2012), the requirement for a second substrate site for NSS function remains in debate.

In addition to helping elucidate the mechanisms of substrate transport, $LeuT_{Aa}$ shares many structural and functional similarities with related monoamine transporters, allowing predictive homology models to be constructed (Rudnick and Wall, 1992; Stephan et al., 1997; Norregaard et al., 1998; Smicun et al., 1999; Mitchell et al., 2004; Beuming et al., 2006, 2008; Zhang and Rudnick, 2006; Forrest et al., 2007, 2008; Huang and Zhan, 2007; Jacobs et al., 2007; Zhou et al., 2007, 2009; Zomot et al., 2007; Erreger et al., 2008; Indarte et al., 2008; Andersen et al., 2009; Tavoulari et al., 2009). For example, homology models built from $LeuT_{Aa}$ have been used to identify putative Cl^- binding sites in serotonin (SERT), dopamine (DAT), and GABA (GAT-1 and GAT-4) transporters (Forrest et al., 2007; Zomot et al., 2007), which predict that Cl^- ions regulate the equilibrium between the open-to-out (substrate binding) and open-to-in (transporting) states (Beuming et al., 2008; Erreger et al., 2008; Forrest et al., 2008; Tavoulari et al., 2009). Homology models have also identified a conserved substrate binding site, equivalent to the leucine site identified in $LeuT_{Aa}$-Leu (Yamashita et al., 2005), which is present across norepinephrine (NET), glycine, tryptophan, and tyrosine transporters (Beuming et al., 2006; Paczkowski et al., 2007).

Here, we used a combination of homology modeling, molecular docking simulations, and site-directed mutagenesis to identify residues affecting NE transport and the binding of its competitive inhibitor nisoxetine (NX), a selective norepinephrine reuptake inhibitor (Jayanthi et al., 1993), in the extracellular mouth of human NET. The NX binding site was found to overlap with the S2 binding site for SSRIs (Zhou et al., 2009) and TCAs (Singh et al., 2007) cocrystallized with $LeuT_{Aa}$, whereas two NE binding sites critical for efficient substrate transport were identified. The apparent high-affinity site for NE (NESS-1) overlapped the leucine binding site (S1) identified in $LeuT_{Aa}$-Leu (Yamashita et al., 005), whereas a lower-affinity site for NE (NESS-2) was identified ~11 Å extracellular to NESS-1. The predicted residues contributing to NE and NX transport and binding were confirmed by site-directed mutagenesis. Our findings support a multistep model of substrate transport by NET.

Materials and Methods

Molecular Modeling and Docking. A molecular model of NET was built using the $LeuT_{Aa}$-Leu (Protein Data Bank 2A65) (Yamashita et al., 2005) cocrystal structure as the template with the program Modeller 9v2 (Fiser and Sali, 2003). All sequence alignments were generated using ClustalW (Larkin et al., 2007) and were corrected manually on the basis of the secondary structure analysis using Phyre (Kelley and Sternberg, 2009) and TMHMM (Krogh et al., 2001) to guide the sequence alignment of the TMHs and low homology regions, especially for ELs (Supplemental Fig. 1). Similar sequence alignment approaches have successfully revealed residues in SLC6 transporters that are likely to regulate substrate binding selectivity and transport mechanisms (Beuming et al., 2006). All resulting homology models were subjected to energy minimization using GROMOS96 (Gunsteren and Berendsen, 1990) with 500 steps of the steepest descent followed by 1000 cycles of conjugated gradient to remove steric incompatibilities. The structural models were evaluated using the online server Verify3D (Bowie et al., 1991) and the Ramachandran plot available from the ProFunc (Laskowski et al., 2005) database. The few residues with unfavorable geometry were relaxed by manually selecting the backbone and side chain atoms with consecutive energy minimization using GROMOS96 or by rigid body refinement using Coot (Emsley and Cowtan, 2004) until the geometry was satisfactory. Assessment of the structure of the NET homology model relative to $LeuT_{Aa}$-Leu (Protein Data Bank 2A65) using the relationship between the protein sequence identity and expected model accuracy (Forrest et al., 2006) supported the sequence alignment (Supplemental Fig. 1) and resulting quality of the NET model generated (Table 1).

We presumed that there would be little conformational change between the substrate-bound and inhibitor-bound states on the basis of the crystallographic parameter B-factors and 3D superimposition of cocrystal structures of $LeuT_{Aa}$ with substrate (Leu) (Yamashita et al., 2005), amino acids (Ala, Gly, Met, and Phe) (Singh et al., 2008), SSRIs (sertraline, *R*-fluoxetine, and *S*-fluoxetine) (Zhou et al., 2009) and TCAs (desipramine, imipramine, and clomipramine) (Singh et al., 2007; Zhou et al., 2007). Therefore, rigid-docking simulation was chosen for searching possible NE and NX binding sites in NET to avoid approach-dependent bias. Structures of NE (Drug Bank database) and its competitive inhibitor NX [generated using the program CORINA (Accelrys, San Diego, CA)] were docked to the NET homology models, including NET and W80A-NET, with three-dimensional fast Fourier transformation docking approaches with high order ($N = 25$) spherical polar Fourier correlation followed by Newton-like energy minimization using the program HEX 5.0 (Ritchie and Kemp, 2000).

Solutions with spatially similar docking orientation (RMSD <3 Å)

TABLE 1

Assessment of the structural relationship between NET model and $LeuT_{Aa}$ crystal structure

The relationship of protein sequence identity and the expected model accuracy based on the backbone RMSD comparison is derived from Forrest et al. (2006) are shown overall and for NESS-1 and NESS-2.

	Residues	No. of Residues	Identity	Expected RMSD to $LeuT_{Aa}$	RMSD to $LeuT_{Aa}$
			%	Å	
Overall	56–582 (5–515)	527/511	27	≥2.5	1.394
NESS-1 versus S1	72–78 (21–27) 156–159 (104–107) 317–323 (253–259) 419–423 (355–359)	23/23	47.8	<2	0.426
NESS-2 versus S2	79–85 (28–34) 160–164 (109–113) 308–316 (244–252) 467–473 (398–404)	28/28	42.8	<2	0.482

were grouped and the lowest energy solution from each group was chosen as a candidate for further analysis. Semiflexible docking simulations using AutoDock Vina (Trott and Olson, 2010) was then performed to optimize the intermolecular interactions, for which both ligands and side chains of the binding site residues predicted by HEX 5.0 were set to be rotatable. The center of the grid map was set as the center of ligands with dimensions of 20 × 20 × 20 Å, covering the predicted binding site, with a searching resolution of 1 Å. The 10 lowest energy solutions for NX and NE docked to NESS-2 of hNET had minimal energies within 5 kcal/mol (Supplemental Fig. 2). All 10 docking solutions for NE and NX were similar (RMSD 1.5 and 1.7 Å, respectively) but nonidentical, with the lowest energy docking solution chosen for detailed analysis. Hydrogen bonds between ligands and NET that are likely to contribute to substrate and inhibitor binding were analyzed using the online server WHAT IF (Vriend, 1990). To determine the influence of mutations on substrate and inhibitor binding, we mutated residues Asp75, Arg81, Trp308, Gln314, Phe316, and Ser419 that were found to form intramolecular interactions in a close proximity to the predicted substrate binding site in the homology models. A NET model derived from the $LeuT_{Aa}$-Trp cocrystal structure failed to dock NE using HEX 5.0.

NET Mutants. Site-direct mutagenesis of human NET was performed as described previously (Paczkowski et al., 2007) using custom-made primers and the QuikChange kit (Stratagene, La Jolla, CA). All mutants were sequenced to verify each mutation. Plasmids of interest were transformed into TOP-10 competent *Escherichia coli* cells (Invitrogen, Carlsbad, CA) for large-scale DNA purification and storage before transfection.

[^{3}H]Norepinephrine Uptake Assays. COS-7 cells (American Type Culture Collection, Manassas, VA) were cultured in Dulbecco's modified Eagle's medium containing 10% fetal bovine serum in 96-well plates. At ~90% confluence, cells were transiently transfected with NET and NET mutant cDNA using 10 μl of FuGENE (Roche, Castle Hill, NSW, Australia) and 2 μg of DNA per 10^6 cells. Twenty-four hours after transfection, 10,000 cells were aliquoted per well in a 96-well plate format for an additional 24-h incubation to obtain a count of ~50,000 cells/well before initiation of the uptake assays. Substrate transport efficiency was determined with increasing concentrations of [^{3}H]norepinephrine ([^{3}H]40.5 Ci/mmol; PerkinElmer Life and Analytical Sciences, Waltham, MA) from 10^{-8} to 5×10^{-6} M in a final volume of 50 μl in 96-well plates and incubated at 37°C for 10 min, followed by two gentle washes using 100 μl of assay buffer [25 mM HEPES, pH 7.4, 125 mM NaCl, 1.2 mM $MgSO_4$, 4.8 mM KCl, 1.2 mM KH_2PO_4, 1.3 mM $CaCl_2$, 5.55 mM *d*-(+)-glucose, and 1 mM ascorbic acid] to remove excess [^{3}H]NE. Nonspecific uptake of [^{3}H]NE by transfected cells was determined in the presence of 200 μM NX. After incubation, cells were lysed using 50 μl of 0.1 M NaOH with gentle shaking for 60 min. The specific [^{3}H]NE uptake was calculated as the difference between the total cellular uptake and the nonspecific uptake. Each experiment was performed in triplicate in at least three separate experiments.

[^{3}H]Nisoxetine Binding Assays. Human NET-transfected (see above) COS-7 cell membrane was used to measure [^{3}H]NX (81.7 Ci/mmol, PerkinElmer Life and Analytical Sciences) binding to NET. Transfected cells were washed and scraped off in the assay buffer containing 1.6 mg/ml protease inhibitor cocktail (Roche Diagnostics, Indianapolis, IN), followed by sonication at 4°C for 25 s. Cell debris was subsequently removed by centrifugation at 465*g* for 10 min, and the membrane was pelleted at 39,000*g* for 30 min at 4°C and finally resuspended in assay buffer. Assays containing 20 μg of total membrane protein per concentration (Bradford assay; Bio-Rad Laboratories, Hercules, CA) and increasing concentrations of [^{3}H]NX from 10^{-10} to 5×10^{-8} M in a final volume of 50 μl were incubated in 96-well plates on ice for 60 min. After incubation, membrane was filtered onto a Filtermat B and washed twice with ice-cold assay buffer to remove unbound [^{3}H]NX using a Filtermat-96 Harvester (PerkinElmer Life and Analytical Sciences). Filtermats were dried in the incubator at 37°C overnight, placed in a TopSeal-A 96-well sleeve (PerkinElmer Life and Analytical Sciences) with Betaplate scintillant (PerkinElmer Life and Analytical Sciences), and sealed before measurement of radioactivity in a MicroBeta counter (PerkinElmer Life and Analytical Sciences). Nonspecific binding of [^{3}H]NX was determined in the presence of 200 μM NX, and specific [^{3}H]NX binding was calculated as the difference between the total cellular and the nonspecific binding. Each experiment was performed in triplicate and repeated four or five times.

Inhibition of [^{3}H]Nisoxetine Binding by Norepinephrine. NE binding affinity was determined from the displacement of [^{3}H]NX from human NET mutants W80A, R81Q, Y84A, L160A, F164A, Q314A, F316A, Y467F, D473A, D473R, and R81D/D473R, which showed no NE uptake and yet retain NX binding function in uptake and binding single-point and saturation assays. The assays were performed as described for [^{3}H]NX binding assays using a fixed concentration of [^{3}H]NX of 3 nM and increasing concentrations of NE from 10^{-14} to 10^{-3} M in 10-fold increments. Each experiment was performed in triplicate and repeated three times.

Inhibition of [^{3}H]Norepinephrine Transport by Nisoxetine. NX affinity was determined from the inhibition of [^{3}H]NE binding to the mutant Y84A-NET to determine the impacts of mutations on NX binding ability. Assays were conducted for mutants L160A and F164A because they showed NX binding (K_d) comparable to that of wild-type NET to support the hypothesis of only one NX binding site in NET. The assays were performed as described for [^{3}H]NE uptake assays using a fixed concentration of [^{3}H]NE of 30 nM and increasing concentrations of NX from 10^{-14} to 10^{-3} M in 10-fold increments. Each experiment was performed in triplicate and repeated three times.

Western Blot. Western blots were prepared for determining total expression using 20 μl of cell membrane (20 μg of total protein) prepared as described for [^{3}H]NX binding assays, mixed with 5 μl of SDS loading dye [0.225 M Tris-HCl, pH 6.8; 50% (v/v) glycerol, 5% (w/v) SDS, 0.05% (w/v) bromphenol blue; 500 mM β-mercaptoethanol], and incubated at room temperature for 10 min before SDS-polyacrylamide gel electrophoresis (PAGE). To separate the native and mutated NET proteins from other cellular proteins, 4 to 12% NuPAGE gels (Invitrogen) were used. After electrophoresis, proteins of interest were transferred to nitrocellulose membrane (Bio-Rad Laboratories). After the transfer, the membranes were blocked in blocking solution (5% (w/v) skim milk) for 1 h, followed by a 45-min incubation with sequence-specific

antibody (1:3000 enzyme/blocking solution ratio; mouse monoclonal antibody to NET targeting N-terminal amino residues 17–33; Abcam Inc., Cambridge, MA). After incubation, the membrane was washed (three 5-min washes) in blocking solution to remove excess primary antibody before the secondary antibody (fluorescently labeled goat anti-mouse IgG (H+L) Alexa Fluor 680; Invitrogen) was added (1:2500 enzyme/blocking solution ratio) and allowed to bind for a further 45 min. Finally, the membranes were washed (three 1-min washes) in a large volume of phosphate buffer solution and scanned using the Odyssey IR imaging system (LI-COR Biosciences, Lincoln, NE). Most membrane proteins generally migrate faster in SDS-PAGE as an artifact of the SDS-lipid micelle complex. The molecular weight of NET wild type in total expression is observed to be ~54 kDa in SDS-PAGE, which corresponds to the literature (Hahn et al., 2003).

Results

Identification of Residues in NESS-2 with Direct or Local Effects on NE Transport and NX Affinity. To identify potential direct interacting residues, we docked NE and NX onto a homology model of NET generated using the $LeuT_{Aa}$-Leu (Yamashita et al., 2005) cocrystal structure as the template. Docking simulations revealed two potential norepinephrine substrate binding sites on NET that we named NESS-1 and NESS-2, as well as a single binding site for NX that overlapped NESS-2. NX was found to occupy a binding pocket similar to that observed previously for TCAs cocrytallised with $LeuT_{Aa}$ (Fig. 1) (Singh et al., 2007), whereas the ~11 Å deeper NESS-1 overlapped the S1 site

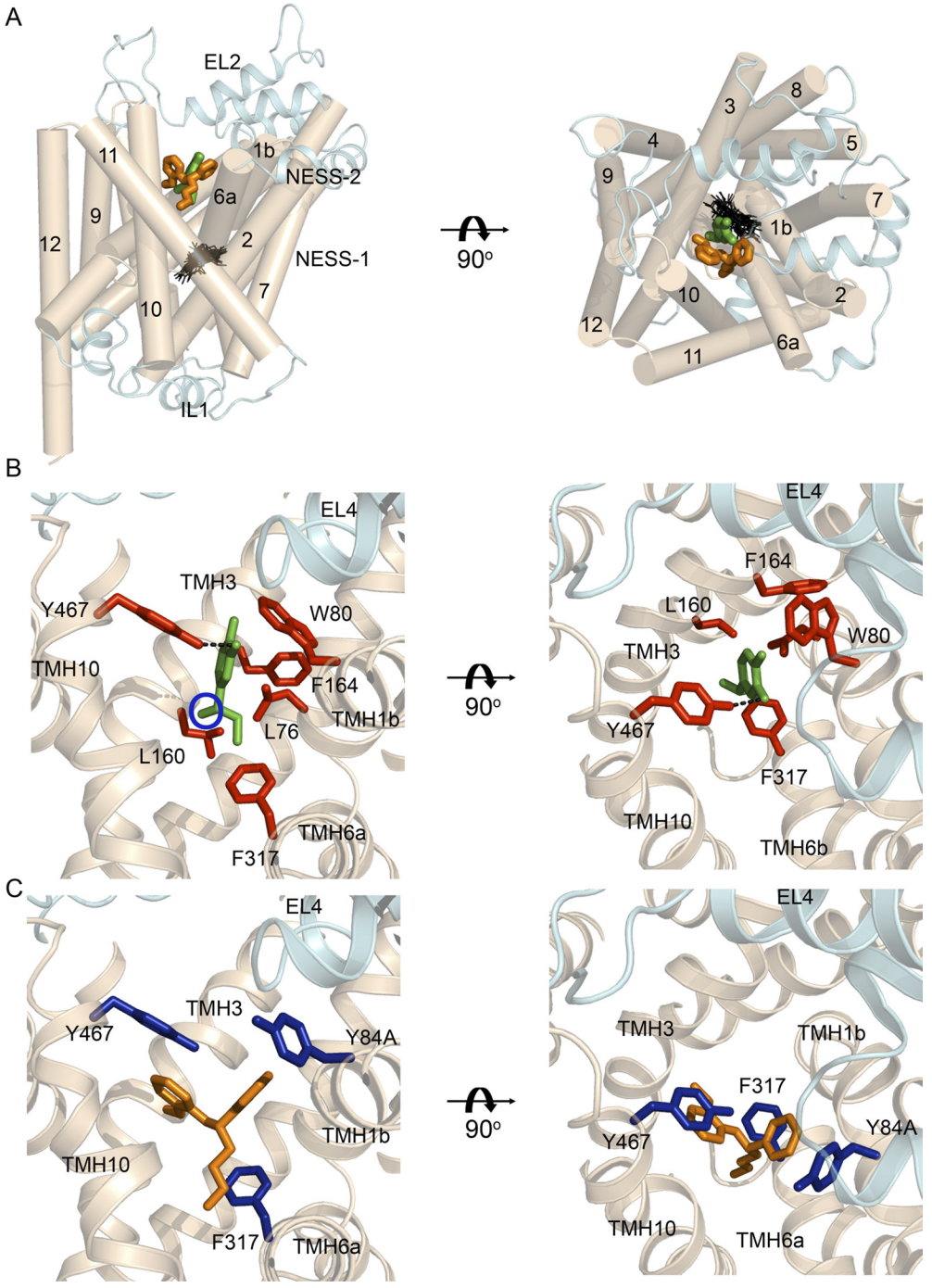

Fig. 1. Homology model of human NET viewed from the side (A, left) or from an extracellular view (A, right). The final docking results of substrate norepinephrine (green) and competitive inhibitor nisoxetine (orange) to the occluded conformation are presented in stick form at NESS-2. The second substrate binding site (NESS-1), which is equivalent to Leu binding site found in $LeuT_{Aa}$ (Yamashita et al., 2005), is indicated with the top 10 energetically favorable docking solutions for NE shown in black (A, left). The specific intermolecular interactions observed for the binding of norepinephrine at NESS-2 (B) and nisoxetine (C) reveal that both binding sites partially overlap and are dominated by hydrophobic interactions. The catecholhydroxyl, the only difference between norepinephrine and dopamine, is indicated by the blue circle (B, left). For clarity, the 3D structures are presented in 50% transparency.

identified for the $LeuT_{Aa}$-Leu cocrystal structure by Yamashita et al. (2005) (Fig. 1A).

Analysis of NE and NX docking results revealed that residues Phe317 (TMH6a) and Tyr317 (TMH10) might contribute to both NX and NE binding; Leu76 and Thr80 (TMH1b) might be NE-specific, whereas Tyr84 (TMH1b) was likely to be NX-specific (Fig. 1, A and C). The direct intermolecular interactions observed to coordinate NE at NESS-2 included a hydrogen bond between the β-hydroxyl of NE and the tyrosine hydroxyl (Tyr317) at a distance of 2.3 Å, a T-stacking π interaction between the two benzene rings of NE and Tyr317 and a cation-π interaction between the positively charged catecholamine of NE and benzene ring of Phe317 at a distance of 2.0 Å (Fig. 1B). Leu76 and Thr80 were predicted to provide additional hydrophobic and van der Waals interactions to coordinate NE binding at distances of 3.2 and 3.8 Å, respectively (Fig. 1B).

Like NE, NX binding was dominated by hydrophobic interactions, for which the methoxybenzene of NX formed a π-π interaction with Tyr317 (~3.1 Å) and the benzene ring of NX formed a T-stacking π interaction with Tyr84 (~3.8 Å). In addition, our model predicted that the nitrogen on the dimethylbenzylamine of NX formed a cation-π interaction with Phe317 (~3.2 Å), as observed previously for NE (Fig. 1B). Further examination of the NET model revealed several hydrophobic residues in the cavity of NET that might indirectly influence NESS-2 residues. Phe164 on TMH3 appeared to form a T-stacking π interaction with Thr80 and a strong hydrophobic interaction with Leu76, suggesting that Phe164 might influence the side chain orientations of Leu76 and Thr80 and indirectly influence their interactions with NE (see above). In addition, Leu160 (TMH3) together with Leu76, Thr80, and Phe164 form a contiguous hydrophobic patch that could interact directly with the catecholbenezene ring of NE (Fig. 1B).

Identification of Additional Residues Predicted to Contribute to the Structure of NESS-2. A number of residues outside NESS-2 were also identified in this NET model that might be expected to influence the structural integrity of NESS-2. Given their prominent positions, Trp308 and Phe316 could act as hydrophobic anchors to stabilize each end of TMH6a, which extends between NESS-2 and NESS-1 (Fig. 2, A and B, respectively), to affect the flexibility and integrity of TMH6a, which has previously been proposed to be essential for substrate transport (Yamashita et al., 2005). In NET, Trp308 is cradled by a hydrophobic patch formed by Pro97 and Leu100 on TMH2, Leu302 on EL3, and Phe528 on TMH11, whereas Phe316 forms an extensive hydrophobic network with Phe101 (T-stacking π) on TMH2 and Ile481, Leu482, and Val485 on TMH10 (Fig. 2B). A second hydrophobic network formed by Phe388 on EL4 interacting with Thr80 on TMH1, Phe167 on TMH3, and Phe409 on TMH8 was also predicted to contribute structurally to the conformation of NESS-2 (Fig. 2C), given that conformational movements of EL4 in $LeuT_{Aa}$ (Singh et al., 2007), GAT-1 (Zomot and Kanner, 2003), DAT (Norregaard et al., 1998), glycine transporter 1b (Ju et al., 2004), and SERT (Mitchell et al., 2004) have been previously demonstrated to accompany substrate and inhibitor binding.

Two residues Asp75 (TMH1b) and Ser419 (TMH8) that might indirectly affect NE transport or NX binding by altering the structural stability of NESS-2 in NET were also identified (Fig. 2D). As observed in the $LeuT_{Aa}$ crystal structure (Yamashita et al., 2005), the electron density of leucine and both Na^+ ion binding sites are well defined, with the leucine and Na^+ ions potentially contributing to this structural stabilization. Asp75 has previously been proposed to substitute for Gly24 in $LeuT_{Aa}$ and coordinate Na^+ ions (Barker et al., 1999; Beuming et al., 2006; Henry et al., 2006; Huang and Zhan, 2007; Indarte et al., 2008), whereas Ser419 contributes to substrate binding in SERT (Andersen et al., 2009). That these residues are fully conserved across monoamine transporters (equivalent to Asp79 and Ser421 in DAT and Asp98 and Ser438 in SERT) further highlights their potential functional significance. On the basis of our modeling, we propose that Asp75 and Ser419 may contribute to the structural stability of NET via ion and substrate binding, as observed in $LeuT_{Aa}$ (Beuming et al., 2006; Henry et al., 2006; Huang and Zhan, 2007; Indarte et al., 2008) and SERT (Andersen et al., 2009). Therefore, mutating Asp75 or Ser419 to alanine destabilizes the NET structure to affect NE transport and/or NX binding.

Identification of Residues Predicted to Gate the Reverse Transport of NE. A hydrogen bond in $LeuT_{Aa}$ (Arg30–Gln250) is disrupted upon TCA binding, allowing the side chain of Arg30 to rotate ~110° where it can form two salt bridges with Asp404 (equivalent to Asp473 in NET) (Singh et al., 2007) that gate the reverse transport of substrate (Chen et al., 2003; Singh et al., 2007; Zhou et al., 2007). Given that Arg30 and Asp404 in $LeuT_{Aa}$ are conserved at equivalent positions across all SLC6 transporters, members of the SLC6 family are likely to share a common gating mechanism. This gating mechanism is also likely to affect NX inhibition, because the amine tail of NX is predicted to prevent the formation of these salt bridges as seen in the $LeuT_{Aa}$-TCA cocrystal structures (Singh et al., 2007). To evaluate this gating mechanism in NET, we assessed NE transport and NX binding in the R81A, R81Q, R81D, Q314A, D473A, D473R, R81Q/Q314R, R81A/Q314A, and R81D/D473R mutants of NET.

Functional Characterization of Docking Predictions. To experimentally test our docking prediction, we created 22 mutants of NET. All mutants were evaluated by immunodetection, binding, and uptake assays to determine the effects on NE transport and NX binding kinetics (Figs. 3 and 4).

Alanine substitutions at four of the five residues in NESS-2 that were predicted to have direct affects on NE and/or NX affinity (W80A, Y84A, F317A, and Y467A) had no significant effect on the levels of NET expression determined by immunodetection, whereas L76A abolished NET expression (Fig. 3A). In support of our predictions, the Y467A and F317A mutants abolished both NE transport and NX binding (Fig. 3B). In contrast to Y467A, Y467F-NET reduced the ability of NE to displace NX by ~3.5-fold, without significantly affecting the apparent Michaelis constant K_m [defined as the extracellular NE concentration required for half-maximal transport velocity (V_{max})] or the NX binding affinity (K_d) (Fig. 4, A and C; Table 2). The Y467F mutant produced an ~9-fold reduction in substrate transport efficiency (V_{max}) that corresponded to the ~6-fold drop in transporter expression determined from the B_{max} for [^{3}H]NX (Table 2). Mutant Y84A reduced NX binding affinity by ~5-fold, which correlated with an ~10-fold reduction in NX inhibition of NE

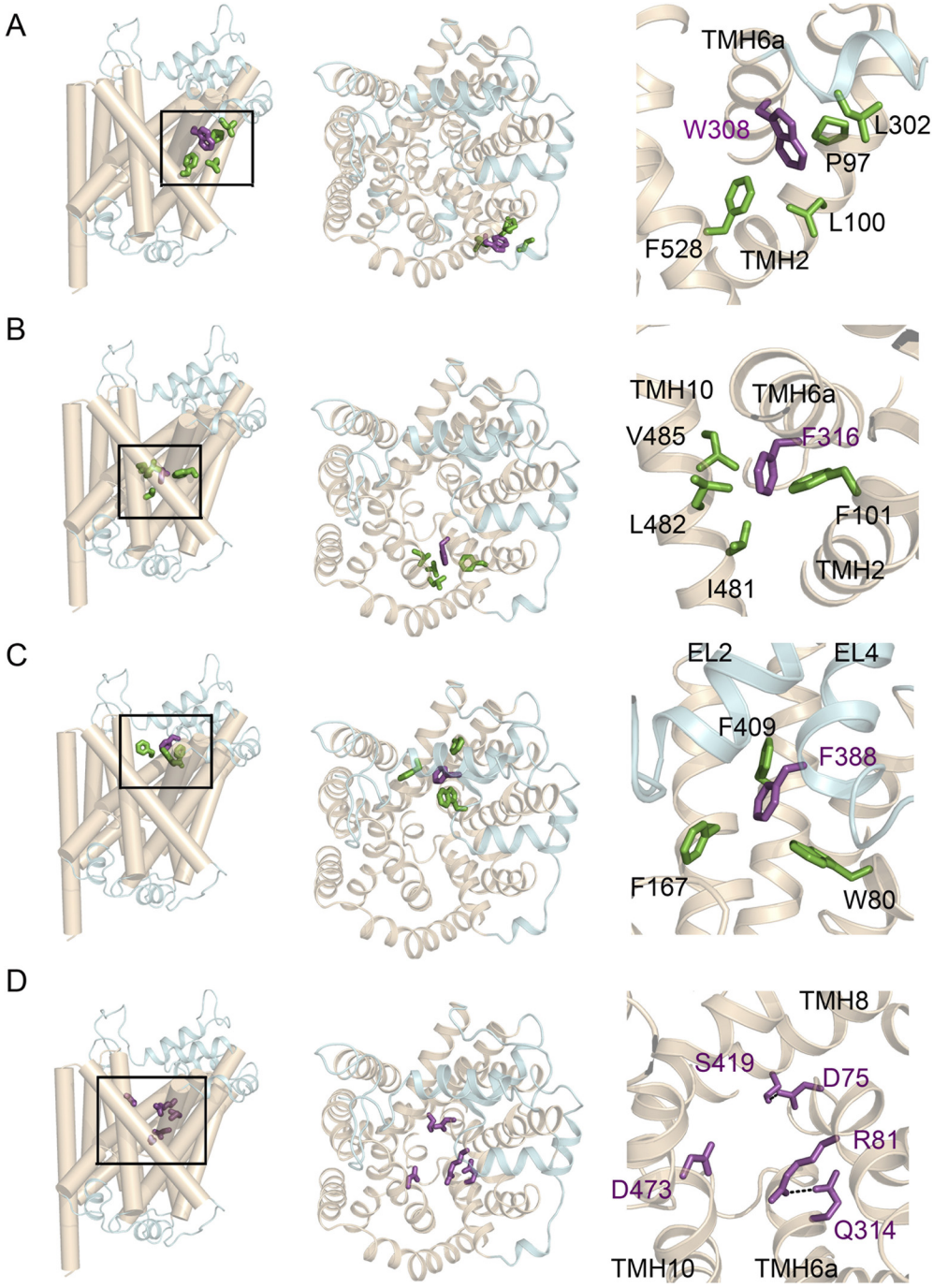

Fig. 2. Residues (purple) predicted to contribute structurally to substrate transport and inhibitor binding in NET. These residues stabilize the integrity of NESS-2 by forming extensive hydrophobic network (A–C) with residues (green), hydrogen bond network, and salt bridge (D) from different TMHs. The overall positions are shown in the left (side view) and middle (top view) panels, with detailed intramolecular interactions presented in the right panel. The 3D structures are presented in 50% transparency.

transport (IC_{50}), without significantly affecting K_m or V_{max} (Fig. 4; Table 2). Finally, mutating the predicted NE-specific residue Thr80 to alanine abolished NE transport (Fig. 4). Of interest, this mutant retained wild-type affinity for NE to displace [^{3}H]NX binding and significantly enhanced (~5-fold) NX affinity (Fig. 4; Table 2).

Phe164 and Leu160 were identified to form part of a contiguous hydrophobic patch in NESS-2, together with Thr80 and Leu76. The F164A mutant caused a 5-fold reduction in K_m (Fig. 4A), indicating that this hydrophobic network is not optimal for NE transport. This mutant did not influence [^{3}H]NX affinity, and the modest ~3-fold reduction in V_{max} corresponded to the observed decrease in transporter expression (B_{max}) (Fig. 4B; Table 2). In contrast, the L160A mutant did not significantly affect any of the measured parameters for NET (Fig. 4; Table 2), indicating that these similar residues are interchangeable.

Asp75 and Ser419 were predicted to play critical roles in stabilizing NET structure via interactions with substrate and the Na^+ ion at NESS-1, respectively, as observed in $LeuT_{Aa}$ (Yamashita et al., 2005). Immunodetection analysis revealed that D75A almost completely abolished NET expression, whereas S419A appeared to cause misfolding that resulted in a decrease in the apparent molecular size of NET (Fig. 3A). These effects on expression account for the almost complete loss of NE transport and NX binding observed for these mutants (Fig. 3).

Residues contributing to the hydrophobic interactions

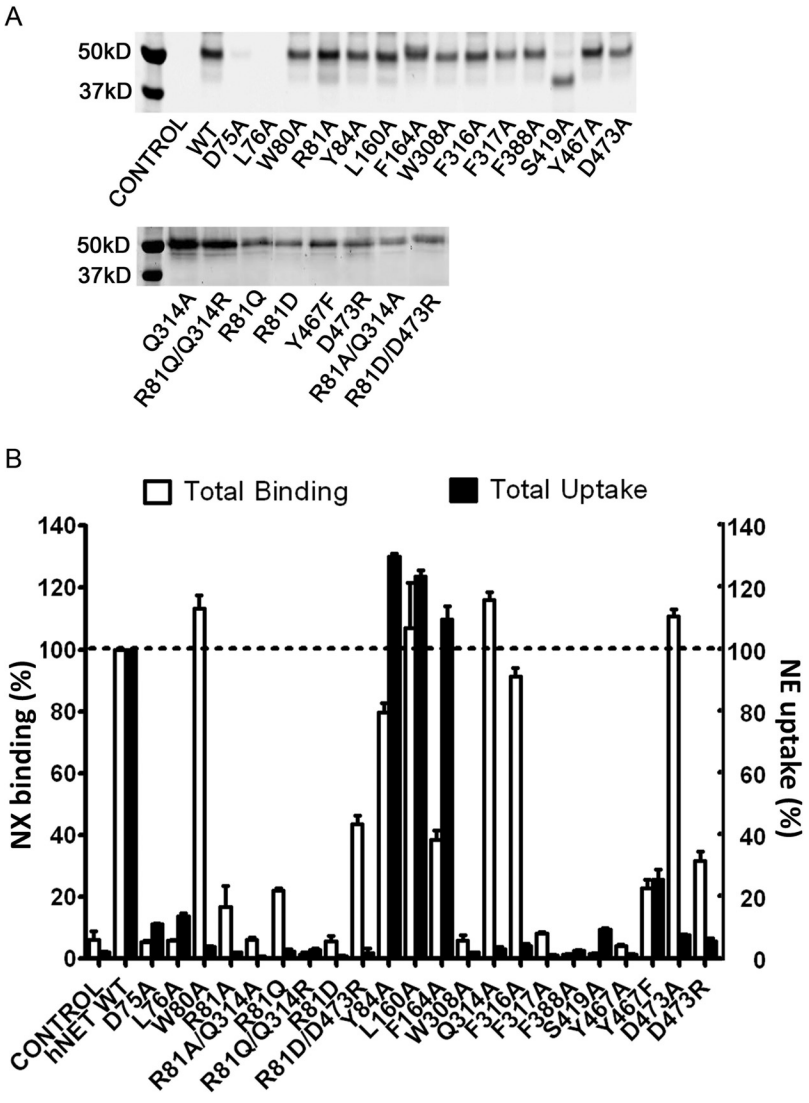

Fig. 3. Immunodetection (A) and single-point normalized NX binding (100% = 1.7 nmol/mg total protein) and NE uptake (100% = 4.2×10^{-14} mol · min^{-1} · $cell^{-1}$) (B) for NET and mutants. The immunodetection indicates that alanine substitution for Asp75 and Leu76 abolishes the transporter expression and the S419A mutant causes misfolding of NET. The effect of each mutation on NX binding (□) and NE uptake (■) are presented as means ± S.E. of at least three independent experiments, each performed in triplicate. h, human; WT, wild type.

associated with NESS-2 and NESS-1 were also investigated. W308A and F388A appeared to express normally but failed to show detectable NE uptake or NX binding, whereas the F316A mutant had significantly impaired NE transport efficiency (~30-fold reduced V_{max}) despite NE K_m and IC_{50} to displace [^{3}H]NX remaining unchanged (Table 2; Figs. 3 and 4).

Despite normal expression (Fig. 3A), all mutations generated at the three proposed extracellular gating residues Arg81, Gln314, and Asp473 significantly diminished or abolished NE uptake. Q314A retained wild-type affinity for NE to displace [^{3}H]NX, whereas D473A produced a ~6-fold reduction (Figs. 3B and 4B). The R81A, R81D, R81A/R314A, and R81Q/Q314R mutants each abolished detectable NE transport and NX binding (Fig. 3B). The R81Q, Q314A, D473A, D473R, and R81D/D473R mutants also failed to generate detectable NE transport, but all bound [^{3}H]NX, albeit mostly at reduced levels. Of interest, despite abolishing transport, the IC_{50} to displace [^{3}H]NX remained unchanged (Table 2), with four mutants (Q314A, D473A, D473R, and R81D/D473R) producing significant (~4-fold) improvements in NX affinity (Fig. 4C; Table 2).

Discussion

The molecular docking simulations and mutagenesis data reported in this study are consistent with two substrate sites being required for NE transport by NET. The first NE substrate site (NESS-2) encountered by NE is located close to the extracellular mouth of NET and is maintained by residues lining the TMH1b-3-6a-8-10 bundle. The second NE substrate site (NESS-1) is positioned ~11 Å below NESS-2 and overlaps the Leu binding site previously identified in the $LeuT_{Aa}$ crystal structure (Yamashita et al., 2005). From analyses of these docking and mutational studies, it appears that NESS-2 might orientate NE for efficient translocation to the deeper site NESS-1. An extracellular substrate binding site has also been identified in SERT and $LeuT_{Aa}$, respectively(Shi et al., 2008; Zhou et al., 2009, 2011; Quick et al., 2012), suggesting that this feature may be common among SLC6 transporters. Of interest, the NX binding site in NET was found to partially overlap NESS-2 but not NESS-1 (Fig. 1) at a location similar to the SSRI and TCA binding site identified in $LeuT_{Aa}$ (Singh et al., 2007; Zhou et al., 2009). Thus, the presence of NESS-2 explains the ability of NX

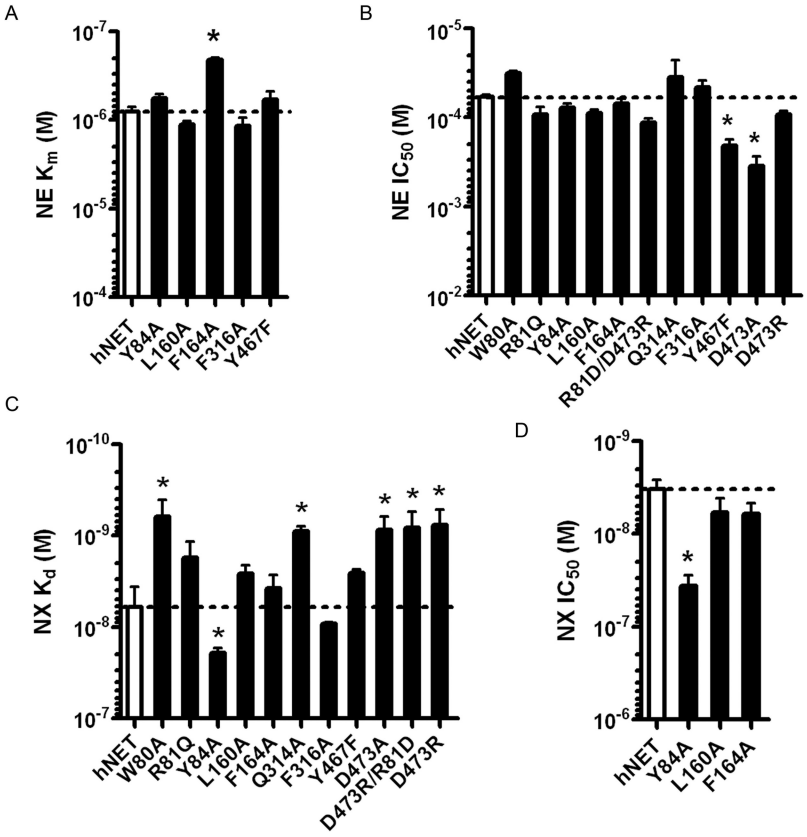

Fig. 4. NE uptake (A) and NX binding saturation (C) and displacement assays (B and D) for wild-type NET and mutants. All mutants were subjected to uptake and binding saturation and displacement assays. Mutants that showed no detectable uptake (up to 5 μM [^{3}H]NE) or binding (50 nM [^{3}H]NX) activity are not shown for clarity. *, mutants that significant affected NE uptake or/and NX binding. Each value represents the mean ± S.E. of at least three independent experiments, each performed in triplicate. Additional kinetics data are summarized in Table 2. h, human.

and TCAs to competitively inhibit NE transport by NET (Jayanthi et al., 1993).

Of the five hydrophobic residues predicted to directly interact with NE and/or NX, mutating four (L76A-NET failed to express) to alanine abolished NE transport (Thr80, Phe317, and Tyr317) or NX binding (Tyr84, Phe317, and Tyr317), suggesting that both NE and NX binding are dominated by extensive hydrophobic interactions. The reduced affinity of NX for the Y84A mutant probably arises because the predicted T-stacking π interaction with NX is disrupted. Loss of both NE transport and NX binding for the F317A mutant supports our modeling prediction that these residues directly coordinate NE and NX binding at NESS-2 via a cation-π interaction. The almost complete loss of NE uptake and NX binding at Y467A-NET, but almost full NE and NX affinity at Y467F-NET, supports the prediction that Tyr317 forms a T-stacking π and hydrogen bond interaction with NE and only a π-π interaction with NX (Fig. 1). The role of Leu76, predicted to directly interact with NE or binding, could not be tested because the alanine substitution unexpectedly abolished NET expression. Given that Leu76 is the first residue of TMH1b and forms an extensive hydrophobic network with Thr80, Leu160, and Phe164 (Fig. 1*B*), a role in stabilizing the structure of NET is proposed in addition to any potential specific role in NE transport or NX binding.

To further understand the pivotal role played by Thr80 in NE transport, we docked NE at a model of W80A-NET (Fig. 5). This simulation revealed a significant shift in NE docking to now completely overlap the NX binding site, which was little altered in this new model (Fig. 5). Despite the loss of NE transport observed experimentally, NE maintained a similar affinity to displace [^{3}H]NX from W80A-NET. This result suggests that the loss of the hydrophobic interactions contributed by Thr80 are compensated for by neighboring hydrophobic residues that reposition NE so that it can no longer be transported. Thus, a single amino acid change can convert NE from a transportable substrate to an antagonist of NX binding to NET. On the basis of this interpretation, we propose that Thr80 is required to correctly position NE at NESS-2 for efficient translocation to NESS-1.

In addition to these direct interactions, we identified five positions (Asp75, Trp308, Phe316, Phe388, and Ser419) that might influence the structure of NESS-2 and -1 (Fig. 2). Consistent with the modeling predictions, mutating these residues to alanine either inhibited NET expression (Asp75), caused protein truncation (Ser419), or abolished NE transport and/or NX binding (Trp308, Phe316, and Phe388). The inhibited NET expression or truncation seen for the D75A and S419A mutants, respectively, presumably arises from the disruption of coordinating Na^+ ions (Barker et al., 1999; Yamashita et al., 2005; Beuming et al., 2006; Henry et al., 2006; Huang and Zhan, 2007; Indarte et al., 2008). The high degree of conservation of both Asp75 and Ser419 in SLC6 transporters suggests that these residues probably play similar structural roles in other SCL6 transporters including SERT (Barker et al., 1999) and $LeuT_{Aa}$ (Yamashita et al., 2005). Residues Trp308 and Phe388 (Fig. 2) were predicted to contribute to the stabilization of the TMH2–6a-10-11 bundle and TMH1b-3-8 and EL4, respectively. Trp308 is located at the end of TMH6a where it could influence the α-helical structure of TMH6a and potentially influence any conformational movement associated with substrate transport.

TABLE 2

NE and NX uptake and affinity at human NET and mutants

Data are means ± S.E.M. of three or four independent experiments separately analyzed in Prism 5. B_{max} and V_{max} are per 20 μg of total cellular protein and ~50,000 cells, respectively.

	Mutation Position	[^{3}H]NX K_d	[^{3}H]NE K_m	NE IC_{50}[a]	NX IC_{50}[a]	[^{3}H]NX B_{max}	[^{3}H]NE V_{max}
		nM		*μM*	*nM*	%	
hNET		4.1 ± 0.5	1.03 ± 0.02	59 ± 3.4	3.4 ± 0.7	100	100
D75A	Loop1a-1b	Low NET expression (~3% of hNET)					
L76A	TMH1b	No detectable NET expression					
W80A	TMH1b	0.8 ± 0.3*	N.D.R.	32 ± 1.7	N.D.	64 ± 7.2	N.D.R.
R81A	TMH1b	N.D.R.	N.D.R.	N.D.	N.D.	N.D.	N.D.
R81D	TMH1b	N.D.R.	N.D.R.	N.D.	N.D.	N.D.	N.D.
R81Q	TMH1b	1.98 ± 0.6	N.D.R.	97 ± 18.2	N.D.	21 ± 5*	N.D.R.
Y84A	TMH1b	19.6 ± 2.5*	0.57 ± 0.6	78 ± 7.6	38 ± 10*	112.7 ± 16.2	81 ± 16
L160A	TMH3	2.7 ± 0.5	1.14 ± 0.1	89 ± 6.8	6.7 ± 2.5	45 ± 7	92.6 ± 28.7
F164A	TMH3	3.9 ± 1.23	0.2 ± 0.01*	70 ± 7.4	6.6 ± 2	29 ± 0.9*	28.5 ± 11*
W308A	TMH6a	N.D.R.	N.D.R.	N.D.	N.D.	N.D.	N.D.
Q314A	TMH6a	0.91 ± 0.1*	N.D.R.	43 ± 17.4	N.D.	69.1 ± 9.65	N.D.R.
F316A	TMH6a	9.3 ± 0.4	1.20 ± 0.26	47 ± 17	N.D.	95.2 ± 1	3.44 ± 0.02*
F317A	TMH6a	N.D.R.	N.D.R.	N.D.	N.D.	N.D.	N.D.
F388A	EL4	N.D.R.	N.D.R.	N.D.	N.D.	N.D.	N.D.
S419A	TMH8	Misfolded NET					
Y467A	TMH10	N.D.R.	N.D.R.	N.D.	N.D.	N.D.	N.D.
Y467F	TMH10	2.56 ± 0.2	0.61 ± 0.13	211 ± 30*	N.D.	16.7 ± 4.9*	10.9 ± 4.9*
D473A	TMH10	0.95 ± 0.3*	N.D.R.	371 ± 82*	N.D.	95 ± 17.6	N.D.R.
D473R	TMH10	0.98 ± 0.4*	N.D.R.	93 ± 8.8	N.D.	35.6 ± 5.8	N.D.R.
R81D/D473R	TMH1b/10	0.87 ± 0.3*	N.D.R.	115 ± 12.2	N.D.	26.6 ± 2.9*	N.D.R.
R81Q/Q314R	TMH1b/6a	N.D.R.	N.D.R.	N.D.	N.D.	N.D.	N.D.
R81A/Q314A	TMH1b/6a	N.D.R.	N.D.R.	N.D.	N.D.	N.D.	N.D.

N.D.R., no detectable response for either specific NX binding up to 200 nM [^{3}H]NX or specific NE uptake up to 5 μM [^{3}H)]NE (three to five separate experiments); N.D., not determined.

* Statistically significant compared with hNET wild type (one-way analysis of variance, $P < 0.05$).

[a] NE IC_{50} determined from displacement of [^{3}H]NX, and NX IC_{50} determined from inhibition of [^{3}H]NE uptake.

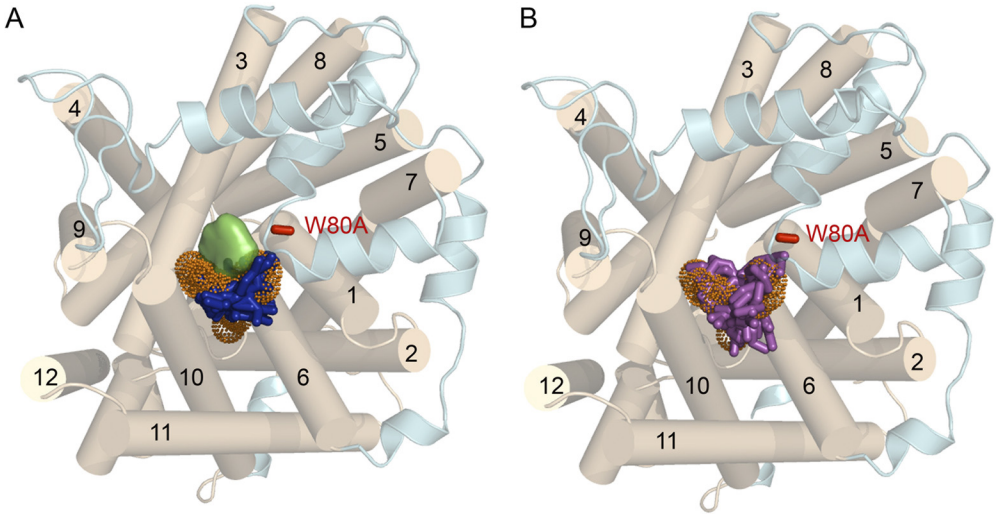

Fig. 5. Docking simulation of NE and NX to the W80A-NET homology model. The identified NE and NX in NET are shown in green half-transparent surface and orange dot mesh, respectively. The top 10 energetically favorable NE (blue) and NX (purple) docking solutions to W80A-NET are presented in stick form in A and B, respectively. The position of residue W80A is presented in red stick. A, docking showed that the initial NE binding site (green) is no longer energetically favorable for binding because of the loss of the hydrophobic interaction provided by Thr80 and that NE binding site is shifted to completely overlap with the NX binding site, in agreement with our NX displacement assays (Fig. 5). B, in contrast, NX docked in the same binding site with slightly different orientation, which may explain the ~5-fold improvement in binding affinity (K_d).

Phe388 is located in EL4, where it could influence the EL4 flexibility, which was previously found to be important for substrate binding (Norregaard et al., 1998; Zomot and Kanner, 2003; Ju et al., 2004; Mitchell et al., 2004; Singh et al., 2007). Finally, the F316A mutant, predicted to also affect the stability of the TMH2–6a-10 bundle, reduced NE transport efficiency to ~3% of that of the wild type, without affecting its K_m or its ability to displace [^{3}H]NX. Reduced NE transport efficiency in the absence of any effect on NESS-2 (NE and NX IC_{50} values unchanged) or NESS-1 (NE K_m unchanged) suggests that this mutation may reduce the rate of the transitions between the open-to-out and open-to-in conformations and implies that the transition to the open-to-in conformation occurs after substrate binds at NESS-1.

On the basis of an analysis of the $LeuT_{Aa}$ crystal structure (Yamashita et al., 2005), an additional three residues, Arg81, Gln314, and Asp473 (Fig. 2D), were predicted to form an extracellular gate in NET that would restrict reverse transport and facilitate forward transport. Consistent with such a role, mutating R81Q, Q314A, D473R, D473A, and R81D/D473R abolished NE uptake with little effect on NX or NE binding affinity. R81A, R81D, R81A/Q314A, and R81Q/Q314R mutants of NET abolished both NX binding and NE transport. Loss of NE transport in the Q314A mutant suggests that the hydrogen bond between Gln314 and Arg81 observed in the $LeuT_{Aa}$ crystal structure (Yamashita et al., 2005) is required to restrict formation of a salt bridge between Arg81 and Asp473 NE before NE binding to NESS-1. Upon NE binding to NESS-1, this

hydrogen bond is broken, allowing Arg81 to reorientate to form a salt bridge with Asp473 to create an extracellular gate. Once formed, this salt bridge is then expected to facilitate structural transitions from the open-to-out to the open-to-in conformation.

K_m and IC_{50} are separate measures of affinity, with the former influenced by transport asymmetry, multiple substrate binding sites, and the multiplicity of conformations in each cycle. However, the large difference between K_m (1 μM) for NE transport and the IC_{50} (59 μM) for NE displacement of NX binding is suggestive of two substrate affinities for NE. This distinct difference was observed across all mutants (Y84A, ~135-fold; L160A, ~80-fold; F164A, ~350-fold; F316A, ~40-fold; and Y467F, ~350-fold) that retained the ability to transport NE. Of interest, the Y467A mutant differentially affected the IC_{50} for NE without affecting its K_m. On the basis of these results, we propose that the low-affinity site determined from NE displacement of NX binding corresponds to NE binding at NESS-2, whereas the K_m for NE is probably driven through higher affinity interactions at NESS-1. This conclusion is consistent with the previously observed competitive interaction between NX and NE (Jayanthi et al., 1993).

The impacts of mutants W80A, R81Q, Q314A, D473A, D473R, and R81D/D473R, which completely abolished substrate transport and yet retained the low-affinity binding interaction, provides experimental support for the presence of two distinct substrate binding sites in NET. The recent studies on $LeuT_{Aa}$ (Shi et al., 2008; Zhao et al., 2011; Quick et al., 2012), human SERT (Sinning et al., 2010), and the carnitine transporter crystal structure (Tang et al., 2010) have also proposed a two-site model for substrate transport.

Taken together, our results support a multistep model for substrate transport by NET as summarized in the scheme shown in Fig. 6. In this model, NE binds first to a low-affinity site at NESS-2 in a substrate binding conformation similar to that observed in the $LeuT_{Aa}$-Leu cocrystal structure (Fig. 6A) (Yamashita et al., 2005). Thr80 in NESS-2 helps orientate NE for efficient NE translocation to the deeper, high-affinity site NESS-1 (Fig. 6B). With NE in NESS-1, a salt bridge then forms between Arg81 and Asp473 (Fig. 6C), as observed in the $LeuT_{Aa}$-Leu cocrystal (Singh et al., 2007; Krishnamurthy and Gouaux, 2012), facilitating a shift to the open-to-in conformation and forward transport of NE and two Na^+ ions (Fig. 6D) (Krishnamurthy and Gouaux, 2012). An extracellular Cl^- ion then probably participates in the final step in substrate transport that releases NE and Na^+ ions intracellularly from the open-to-in confirmation (Fig. 6D), before an intracellular Cl^- ion facilitates the structural reorganization of NET back to the substrate binding conformation (Erreger et al., 2008; Tavoulari et al., 2009). Because we have established that NESS-2 is above NESS-1, it is likely that NE must bind first at NESS-2 before it is translocated to the higher affinity NESS-1 and transported.

These studies of NET transport also provide insights into the structural features contributing to substrate selectivity. Our docking studies also show that the catecholbenzene, catecholamine, and β-hydroxyl of NE form intermolecular interactions with NET, whereas the catecholhydroxyl does not, suggesting that catecholhydroxyl may not be essential for transport. This observation can explain why NET can transport both NE and DA (Buck and Amara, 1994; Carboni and Silvagni, 2004), which differ only by this catecholhydroxyl (Fig. 1B). In contrast, DAT is incapable of transporting NE, suggesting that the size of the catechol tail is a key determinant of DAT monoamine substrate specificity.

In conclusion, we have used the $LeuT_{Aa}$-Leu crystal structure as a template to identify a second extracellular NE binding site named NESS-2, which is essential for efficient substrate transport by NET. Mutating 14 of the 15 residues identified from modeling produced effects on substrate transport and/or selective norepinephrine reuptake inhibitor binding, confirming the predictive value of NET models built from $LeuT_{Aa}$ crystal structures. The residues identified here are mostly conserved across monoamine transporters, suggesting that they probably have similar roles in related SLC6 transporters. The identification of new residues in NESS-2 that directly interact with substrate NE and/or NX may facilitate the development of new monoamine transporter inhibitors.

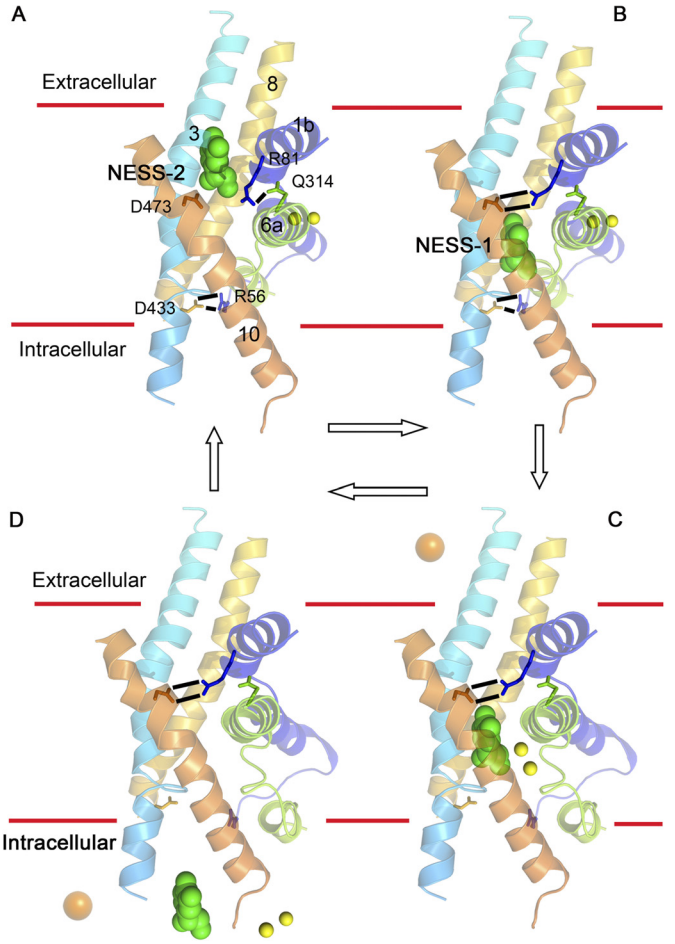

Fig. 6. A schematic diagram of the proposed substrate transport mechanism for NET. In this model, NE (green) first transitions from a low-affinity site, NESS-2 (A), to a deeper high-affinity site, NESS-1 (B). With NE in NESS-1, a salt bridge forms between Arg81 and Asp473 and an extracellular Cl^- ion binds (orange sphere), facilitating the forward transport of NE and two Na^+ ions (yellow) (E). To complete the cycle, an intracellular Cl^- ion binds to NET and facilitates a conformational change(s) from the transporting to the substrate binding conformation (A). For clarity, only the core TMHs are shown.

Acknowledgments

We thank Dr. Lotten Ragnarsson-McGrath for molecular biology advice and help constructing difficult mutations.

Authorship Contributions

Participated in research design: Wang, Shaikh, and Lewis.
Conducted experiments: Wang, Shaikh, and Ramu.
Performed data analysis: Wang, Shaikh, and Lewis.
Wrote or contributed to the writing of the manuscript: Wang and Lewis.

References

Amara SG and Sonders MS (1998) Neurotransmitter transporters as molecular targets for addictive drugs. *Drug Alcohol Depend* **51:**87–96.
Andersen J, Kristensen AS, Bang-Andersen B, and Stromgaard K (2009) Recent advances in the understanding of the interaction of antidepressant drugs with serotonin and norepinephrine transporters. *Chem Commun (Camb)* **25:**3677–3692.
Barker EL, Moore KR, Rakhshan F, and Blakely RD (1999) Transmembrane domain I contributes to the permeation pathway for serotonin and ions in the serotonin transporter. *J Neurosci* **19:**4705–4717.
Beuming T, Kniazeff J, Bergmann ML, Shi L, Gracia L, Raniszewska K, Newman AH, Javitch JA, Weinstein H, Gether U, et al. (2008) The binding sites for cocaine and dopamine in the dopamine transporter overlap. *Nat Neurosci* **11:**780–789.
Beuming T, Shi L, Javitch JA, and Weinstein H (2006) A comprehensive structure-based alignment of prokaryotic and eukaryotic neurotransmitter/Na^+ symporters (NSS) aids in the use of the LeuT structure to probe NSS structure and function. *Mol Pharmacol* **70:**1630–1642.
Bowie JU, Lüthy R, and Eisenberg D (1991) A method to identify protein sequences that fold into a known three-dimensional structure. *Science* **253:**164–170.
Brust A, Palant E, Croker DE, Colless B, Drinkwater R, Patterson B, Schroeder CI, Wilson D, Nielsen CK, Smith MT, et al. (2009) chi-Conopeptide pharmacophore development: toward a novel class of norepinephrine transporter inhibitor (Xen2174) for pain. *J Med Chem* **52:**6991–7002.
Buck KJ and Amara SG (1994) Chimeric dopamine-norepinephrine transporters delineate structural domains influencing selectivity for catecholamines and 1-methyl-4-phenylpyridinium. *Proc Natl Acad Sci USA* **91:**12584–12588.
Carboni E and Silvagni A (2004) Dopamine reuptake by norepinephrine neurons: exception or rule? *Crit Rev Neurobiol* **16:**121–128.
Chen J, Lu G, Lin J, Davidson AL, and Quiocho FA (2003) A tweezers-like motion of the ATP-binding cassette dimer in an ABC transport cycle. *Mol Cell* **12:**651–661.
Chen NH, Reith ME, and Quick MW (2004) Synaptic uptake and beyond: the sodium- and chloride-dependent neurotransmitter transporter family SLC6. *Pflugers Arch* **447:**519–531.
Dougherty DD, Bonab AA, Spencer TJ, Rauch SL, Madras BK, and Fischman AJ (1999) Dopamine transporter density in patients with attention deficit hyperactivity disorder. *Lancet* **354:**2132–2133.
Emsley P and Cowtan K (2004) Coot: model-building tools for molecular graphics. *Acta Crystallogr D Biol Crystallogr* **60:**2126–2132.
Erreger K, Grewer C, Javitch JA, and Galli A (2008) Currents in response to rapid concentration jumps of amphetamine uncover novel aspects of human dopamine transporter function. *J Neurosci* **28:**976–989.
Fiser A and Sali A (2003) Modeller: generation and refinement of homology-based protein structure models. *Methods Enzymol* **374:**461–491.
Forrest LR, Tang CL, and Honig B (2006) On the accuracy of homology modeling and sequence alignment methods applied to membrane proteins. *Biophys J* **91:**508–517.
Forrest LR, Tavoulari S, Zhang YW, Rudnick G, and Honig B (2007) Identification of a chloride ion binding site in Na^+/Cl^--dependent transporters. *Proc Natl Acad Sci USA* **104:**12761–12766.
Forrest LR, Zhang YW, Jacobs MT, Gesmonde J, Xie L, Honig BH, and Rudnick G (2008) Mechanism for alternating access in neurotransmitter transporters. *Proc Natl Acad Sci USA* **105:**10338–10343.
Gunsteren WF von and Berendsen HJC (1990) Computer simulation of molecular dynamics: methodology, applications, and perspectives in chemistry. *Angew Chem Int Ed Eng* **29:**992–1023.
Hahn MK, Robertson D, and Blakely RD (2003) A mutation in the human norepinephrine transporter gene (SLC6A2) associated with orthostatic intolerance disrupts surface expression of mutant and wild-type transporters. *J Neurosci* **23:**4470–4478.
Henry LK, Defelice LJ, and Blakely RD (2006) Getting the message across: a recent transporter structure shows the way. *Neuron* **49:**791–796.
Huang X and Zhan CG (2007) How dopamine transporter interacts with dopamine: insights from molecular modeling and simulation. *Biophys J* **93:**3627–3639.
Indarte M, Madura JD, and Surratt CK (2008) Dopamine transporter comparative molecular modeling and binding site prediction using the LeuT(Aa) leucine transporter as a template. *Proteins* **70:**1033–1046.
Jacobs MT, Zhang YW, Campbell SD, and Rudnick G (2007) Ibogaine, a noncompetitive inhibitor of serotonin transport, acts by stabilizing the cytoplasm-facing state of the transporter. *J Biol Chem* **282:**29441–29447.
Jayanthi LD, Prasad PD, Ramamoorthy S, Mahesh VB, Leibach FH, and Ganapathy V (1993) Sodium- and chloride-dependent, cocaine-sensitive, high-affinity binding of nisoxetine to the human placental norepinephrine transporter. *Biochemistry* **32:**12178–12185.
Jeon B, Kim JM, Jeong JM, Kim KM, Chang YS, Lee DS, and Lee MC (1998) Dopamine transporter imaging with [^{123}I]-β-CIT demonstrates presynaptic nigrostriatal dopaminergic damage in Wilson's disease. *J Neurol Neurosurg Psychiatry* **65:**60–64.
Ju P, Aubrey KR, and Vandenberg RJ (2004) Zn^{2+} inhibits glycine transport by glycine transporter subtype 1b. *J Biol Chem* **279:**22983–22991.
Kelley LA and Sternberg MJ (2009) Protein structure prediction on the Web: a case study using the Phyre server. *Nat Protoc* **4:**363–371.
Kim HJ, Im JH, Yang SO, Moon DH, Ryu JS, Bong JK, Nam KP, Cheon JH, Lee MC, and Lee HK (1997) Imaging and quantitation of dopamine transporters with iodine-^{123}-IPT in normal and Parkinson's disease subjects. *J Nucl Med* **38:**1703–1711.
Klimek V, Stockmeier C, Overholser J, Meltzer HY, Kalka S, Dilley G, and Ordway GA (1997) Reduced levels of norepinephrine transporters in the locus coeruleus in major depression. *J Neurosci* **17:**8451–8458.
Krishnamurthy H and Gouaux E (2012) X-ray structures of LeuT in substrate-free outward-open and apo inward-open states. *Nature* **481:**469–474.
Krishnamurthy H, Piscitelli CL, and Gouaux E (2009) Unlocking the molecular secrets of sodium-coupled transporters. *Nature* **459:**347–355.
Krogh A, Larsson B, von Heijne G, and Sonnhammer EL (2001) Predicting transmembrane protein topology with a hidden Markov model: application to complete genomes. *J Mol Biol* **305:**567–580.
Larkin MA, Blackshields G, Brown NP, Chenna R, McGettigan PA, McWilliam H, Valentin F, Wallace IM, Wilm A, Lopez R, et al. (2007) Clustal W and Clustal X version 2. *Bioinformatics* **23:**2947–2948.
Laskowski RA, Watson JD, and Thornton JM (2005) ProFunc: a server for predicting protein function from 3D structure. *Nucleic Acids Res* **33:**W89–W93.
Masson J, Sagné C, Hamon M, and El Mestikawy S (1999) Neurotransmitter transporters in the central nervous system. *Pharmacol Rev* **51:**439–464.
Mitchell SM, Lee E, Garcia ML, and Stephan MM (2004) Structure and function of extracellular loop 4 of the serotonin transporter as revealed by cysteine-scanning mutagenesis. *J Biol Chem* **279:**24089–24099.
Nielsen CK, Lewis RJ, Alewood D, Drinkwater R, Palant E, Patterson M, Yaksh TL, McCumber D, and Smith MT (2005) Anti-allodynic efficacy of the chi-conopeptide, Xen2174, in rats with neuropathic pain. *Pain* **118:**112–124.
Norregaard L, Frederiksen D, Nielsen EO, and Gether U (1998) Delineation of an endogenous zinc-binding site in the human dopamine transporter. *EMBO J* **17:**4266–4273.
Paczkowski FA, Sharpe IA, Dutertre S, and Lewis RJ (2007) chi-Conotoxin and tricyclic antidepressant interactions at the norepinephrine transporter define a new transporter model. *J Biol Chem* **282:**17837–17844.
Piscitelli CL, Krishnamurthy H, and Gouaux E (2010) Neurotransmitter/sodium symporter orthologue LeuT has a single high-affinity substrate site. *Nature* **468:**1129–1132.
Quick M, Shi L, Zehnpfennig B, Weinstein H, and Javitch JA (2012) Experimental conditions can obscure the second high-affinity site in LeuT. *Nat Struct Mol Biol* **19:**207–211.
Quick M, Winther AM, Shi L, Nissen P, Weinstein H, and Javitch JA (2009) Binding of an octylglucoside detergent molecule in the second substrate (S2) site of LeuT establishes an inhibitor-bound conformation. *Proc Natl Acad Sci USA* **106:**5563–5568.
Ritchie DW and Kemp GJ (2000) Protein docking using spherical polar Fourier correlations. *Proteins* **39:**178–194.
Ritz MC, Lamb RJ, Goldberg SR, and Kuhar MJ (1987) Cocaine receptors on dopamine transporters are related to self-administration of cocaine. *Science* **237:**1219–1223.
Rudnick G and Wall SC (1992) The molecular mechanism of "ecstasy" [3,4-methylenedioxy-methamphetamine (MDMA)]: serotonin transporters are targets for MDMA-induced serotonin release. *Proc Natl Acad Sci USA* **89:**1817–1821.
Sharpe IA, Gehrmann J, Loughnan ML, Thomas L, Adams DA, Atkins A, Palant E, Craik DJ, Adams DJ, Alewood PF, et al. (2001) Two new classes of conopeptides inhibit the α_1-adrenoceptor and noradrenaline transporter. *Nat Neurosci* **4:**902–907.
Shi L, Quick M, Zhao Y, Weinstein H, and Javitch JA (2008) The mechanism of a neurotransmitter:sodium symporter—inward release of Na^+ and substrate is triggered by substrate in a second binding site. *Mol Cell* **30:**667–677.
Singh SK, Piscitelli CL, Yamashita A, and Gouaux E (2008) A competitive inhibitor traps LeuT in an open-to-out conformation. *Science* **322:**1655–1661.
Singh SK, Yamashita A, and Gouaux E (2007) Antidepressant binding site in a bacterial homologue of neurotransmitter transporters. *Nature* **448:**952–956.
Sinning S, Musgaard M, Jensen M, Severinsen K, Celik L, Koldsø H, Meyer T, Bols M, Jensen HH, Schiøtt B, et al. (2010) Binding and orientation of tricyclic antidepressants within the central substrate site of the human serotonin transporter. *J Biol Chem* **285:**8363–8374.
Smicun Y, Campbell SD, Chen MA, Gu H, and Rudnick G (1999) The role of external loop regions in serotonin transport. Loop scanning mutagenesis of the serotonin transporter external domain. *J Biol Chem* **274:**36058–36064.
Stephan MM, Chen MA, Penado KM, and Rudnick G (1997) An extracellular loop region of the serotonin transporter may be involved in the translocation mechanism. *Biochemistry* **36:**1322–1328.
Tang L, Bai L, Wang WH, and Jiang T (2010) Crystal structure of the carnitine transporter and insights into the antiport mechanism. *Nat Struct Mol Biol* **17:**492–496.
Tavoulari S, Forrest LR, and Rudnick G (2009) Fluoxetine (Prozac) binding to serotonin transporter is modulated by chloride and conformational changes. *J Neurosci* **29:**9635–9643.
Trott O and Olson AJ (2010) AutoDock Vina: Improving the speed and accuracy of docking with a new scoring function, efficient optimization, and multithreading. *J Comput Chem* **31:**455–461.

Vriend G (1990) WHAT IF: a molecular modeling and drug design program. *J Mol Graph* **8:**52–56, 29.
Wang H, Elferich J, and Gouaux E (2012) Structures of LeuT in bicelles define conformation and substrate binding in a membrane-like context. *Nat Struct Mol Biol* **19:**212–219.
Wong DF, Harris JC, Naidu S, Yokoi F, Marenco S, Dannals RF, Ravert HT, Yaster M, Evans A, Rousset O, et al. (1996) Dopamine transporters are markedly reduced in Lesch-Nyhan disease in vivo. *Proc Natl Acad Sci USA* **93:**5539–5543.
Yamashita A, Singh SK, Kawate T, Jin Y, and Gouaux E (2005) Crystal structure of a bacterial homologue of Na^+/Cl^--dependent neurotransmitter transporters. *Nature* **437:**215–223.
Zhang YW and Rudnick G (2006) The cytoplasmic substrate permeation pathway of serotonin transporter. *J Biol Chem* **281:**36213–36220.
Zhao Y, Terry DS, Shi L, Quick M, Weinstein H, Blanchard SC, and Javitch JA (2011) Substrate-modulated gating dynamics in a Na^+-coupled neurotransmitter transporter homologue. *Nature* **474:**109–113.
Zhou Z, Zhen J, Karpowich NK, Goetz RM, Law CJ, Reith ME, and Wang DN (2007) LeuT-desipramine structure reveals how antidepressants block neurotransmitter reuptake. *Science* **317:**1390–1393.
Zhou Z, Zhen J, Karpowich NK, Law CJ, Reith ME, and Wang DN (2009) Antidepressant specificity of serotonin transporter suggested by three LeuT-SSRI structures. *Nat Struct Mol Biol* **16:**652–657.
Zomot E, Bendahan A, Quick M, Zhao Y, Javitch JA, and Kanner BI (2007) Mechanism of chloride interaction with neurotransmitter:sodium symporters. *Nature* **449:**726–730.
Zomot E and Kanner BI (2003) The interaction of the γ-aminobutyric acid transporter GAT-1 with the neurotransmitter is selectively impaired by sulfhydryl modification of a conformationally sensitive cysteine residue engineered into extracellular loop IV. *J Biol Chem* **278:**42950–42958.

Address correspondence to: Professor Richard J. Lewis, Institute for Molecular Bioscience, The University of Queensland, 306 Carmody Rd., St. Lucia, Brisbane, QLD 4072, Australia. E-mail: r.lewis@imb.uq.edu.au